

Modeling the near-wake of a vertical-axis cross-flow turbine with 2-D and 3-D RANS

Peter Bachant^{1, a)} and Martin Wosnik¹

Center for Ocean Renewable Energy, University of New Hampshire, Durham, NH

(Dated: 15 May 2022)

The near-wake of a vertical-axis cross-flow turbine (CFT) was modeled numerically via blade-resolved $k-\omega$ SST and Spalart–Allmaras RANS models in two and three dimensions. Results for each case are compared with experimental measurements of the turbine shaft power, overall drag, mean velocity, turbulence kinetic energy, and momentum transport terms in the near-wake at one diameter downstream. It was shown that 2-D simulations overpredict turbine loading and do not resolve mean vertical momentum transport, which plays an important role in the near-wake’s momentum balance. The 3-D simulations fared better at predicting performance, with the Spalart–Allmaras model predictions being closest to the experiments. The SST model more accurately predicted the turbulence kinetic energy while the Spalart–Allmaras model more closely matched the momentum transport terms in the near-wake. These results show the potential of blade-resolved RANS as a design tool and a way to “interpolate” experimental flow field measurements.

^{a)}pxl3@unh.edu

I. INTRODUCTION

In the pursuit of a fully sustainable energy profile, cross-flow (often vertical-axis) turbines (CFTs) can still play a role. Despite extensive research and development in the 1970s through the early 1990s by groups like Sandia National Labs in the US¹ and the National Research Council in Canada², the vertical-axis cross-flow Darrieus turbines were all but abandoned for large scale commercial terrestrial wind power. Today, however, with the development of marine hydrokinetic (MHK) energy devices, CFTs are at the forefront, with the first grid-connected commercial device being a horizontal-axis CFT manufactured and installed by ORPC in Cobscook Bay, Maine³. CFTs are also being examined for small-scale onshore wind in urban areas⁴, offshore floating wind farms^{5,6}, and onshore wind farms where power output per unit land area is of interest⁷.

Despite the development of many simple engineering models based on blade element momentum or vortex methods, it remains difficult to predict the performance of cross-flow turbines (CFTs, often vertical-axis turbines or VATs) in all cases—namely when solidity, or blade chord-to-radius ratio is high—a common characteristic of smaller rotors, and those designed for marine hydrokinetic (MHK) applications. With computing power becoming evermore available and affordable, computational fluid dynamics (CFD) has become an attractive method for predicting the performance of cross-flow turbines since it only requires that turbulence be modeled, i.e., the physics can be described from theoretical true first principles by solving the Navier–Stokes equations using a boundary layer resolving body-fitted grid. However, CFD can be computationally expensive when done in three dimensions, which may be necessary in some cases.

There are many examples in the literature of 2-D cross-flow turbine simulations with widely varying results. Balduzzi et al.⁸ provides a summary of recent efforts and an attempt to standardize a methodology for using Reynolds-averaged Navier–Stokes (RANS) to correctly predict performance of a 2-D CFT. Howell et al.⁹, performed both 2-D and 3-D simulations of a high solidity cross-flow turbine using a $k-\epsilon$ renormalization group (RNG) turbulence model. The results from the 2-D simulations over-predicted power coefficient, while the 3-D case matched well with wind tunnel measurements near the tip speed ratio of maximum power. In general, 3-D simulations are less common, but have begun to appear more frequently recently—a testament to the progress towards higher computing power.

Author	Turbulence modeling	Perf. val.	Wake val.
Alaimo et al. ¹¹	$k-\epsilon$	N/A	N/A
Marsh et al. ¹²	SST	Reference ¹³	N/A
Orlandi et al. ¹⁴	SST	References ^{15,16}	N/A
Lam & Peng ¹⁷	SST RANS & IDDES	N/A	Reference ¹⁸
Nini et al. ¹⁹	Spalart–Allmaras	N/A	Reference ²⁰
Boudreau & Dumas ²¹	DDES	N/A	N/A
Li et al. ²²	SST & Smagorinsky–Lilly LES	Reference ²³	N/A
Howell et al. ⁹	$k-\epsilon$ RNG	Reference ⁹	N/A

TABLE I: Selected 3-D blade-resolved cross-flow turbine simulations reported in the literature, turbulence modeling employed, and performance and/or wake studies used for validation. Note the Li et al. study used periodic boundary conditions and is technically considered 2.5-D.

An overview of 3-D blade-resolved cross-flow turbine simulations reported in the literature is presented in Table I. The $k-\omega$ SST RANS turbulence model is shown to be a popular choice due to its success in predicting flows with adverse pressure gradients and separation¹⁰. Higher fidelity methods that resolve the large scales of turbulence, such as large-eddy and detached-eddy simulation have also been used. Note that for all the studies listed, model validation was either done for performance or wake predictions—not both—and in some case omitted entirely.

Modeling the boundary layer flows on cross-flow turbine blades is essential to predicting the blade loading. This flow condition presents a challenge due to the dynamically changing inflow velocity and angle of attack—which often exceeds static stall values and causes dynamic stall. Furthermore, the ability to predict the occurrence and interdependence of boundary layer transition to turbulence and separation can have dramatic influence on the blade loading and therefore the predicted turbine power output. These challenges present significant obstacles to the prospect of using CFD to replace wind tunnel or tank testing of physical models.

To date, little computational work has been done to attempt to design arrays of CFTs, despite their prospects for closer spacing compared with axial-flow turbines (AFTs). For ex-

ample, Araya et al.²⁴ modeled the flow through a VAT array using “leaky Rankine body” potential flow singularities, which was able to rank relative—though not absolute—performance of array configurations. Goude and Agren²⁵ used a 2-D vortex method to simulate a farm of cross-flow turbines, though this was not validated with experiments. Durrani et al.²⁶ used 2-D CFD to model a group of cross-flow turbines, observing higher power output for a staggered configuration, but also did not compare with experimental results. Giorgetti et al.²⁷ took a similar approach for 2-D array analysis using turbine pairs inspired by Dabiri⁷, but again experimental validation was not performed. Li and Calisal²⁸ used a 3-D vortex line method to show mutually improved power output from two adjacent turbines, though the simulations over-predicted the effects compared with experiments. Antheaume et al.²⁹ used a blade element approach coupled with a 3-D RANS solver to also show how close spacing can improve power output of CFTs.

In this study we set out to model the performance and near-wake of the high solidity University of New Hampshire Reference Vertical Axis Turbine (UNH-RVAT) using the Reynolds-averaged Navier–Stokes equations discretized via the finite volume method. Though studies in the literature generally focus on predicting the turbine loading and the local blade boundary layer, we seek to model both this and the larger scale flow produced by the rotor, i.e., the near-wake, which is of interest for this particular turbine since it has been shown experimentally that the near-wake’s momentum and energy transport processes are dominated by vertical advection³⁰. It logically follows that a 2-D simulation, which omits the vertical dimension, would not correctly predict wake recovery and turbine–turbine interaction. However, it is of interest to determine how wrong a 2-D model may be, since the computational feasibility is attractive.

It is assumed that if the turbine power output and near-wake predictions from the numerical model match those of the experiments, the flow field can be inspected in greater detail, i.e., that the experiments will have been “interpolated.” This will provide access to unmeasured quantities, e.g., pressure, and allow inspection into where the dominant flow structures originate. This will ultimately help develop and evaluate low-order wake generator models for use in turbine array modeling. In summary, the questions we hope to answer here are:

1. Can 2-D RANS be used for individual turbine and/or array design?

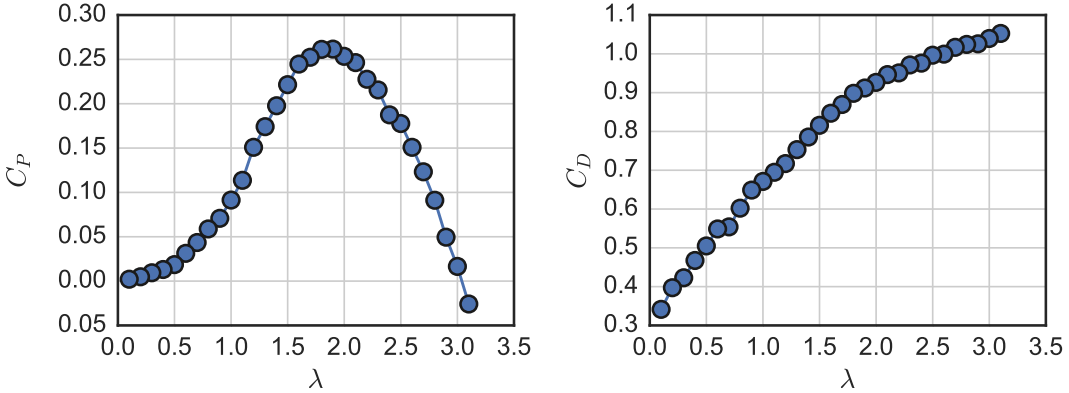


FIG. 1: Mean rotor power (left) and drag (right) coefficient curves from the tow tank experiments³³.

2. How accurately can 3-D RANS predict performance?
3. Can 3-D RANS “interpolate” the experimental results and provide insight to develop new low-order wake generators to represent CFTs?
4. Does 3-D RANS realize the correct proportions of wake recovery mechanisms, i.e., are the 3-D blade-resolved results a good “target” for those a low-order model should produce?

II. NUMERICAL SETUP

In this study the UNH-RVAT baseline tow tank experiment was simulated using a mean rotor tip speed ratio $\lambda = 1.9$, which corresponds to the maximum measured power coefficient; cf. Figure 1. The tow speed or free stream velocity $U_\infty = 1.0$ m/s gives a turbine diameter Reynolds number $Re_D \approx 10^6$, which corresponds to the Re -independent state for both performance and near-wake characteristics, as determined from previous experimental measurements^{31,32}.

The turbines CAD geometry was prepared or “cleaned” for CFD by removing details determined to be unnecessary, e.g., screw heads and axial shaft grooves, which would complicate the meshing process and contribute very little to the overall loading or flow modulation. A drawing of the physically and numerically modeled geometries is presented in Figure 2.

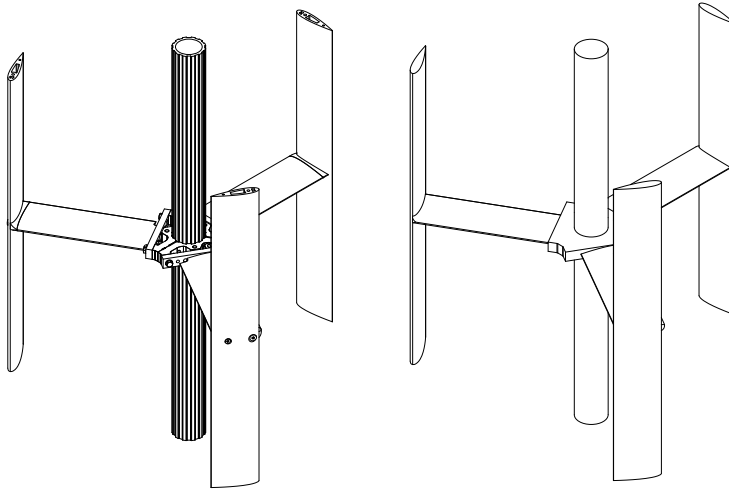


FIG. 2: CAD drawings of the UNH-RVAT cross-flow turbine as designed (left) and cleaned for simulation (right).

To close the RANS equations, two different turbulence models were used—Menter’s $k-\omega$ SST³⁴ and the Spalart–Allmaras (SA) one equation model³⁵. Both closures use the eddy-viscosity approach—the SA employing a single additional scalar transport equation and the SST two. The SST model was chosen due to its prominence in the literature for simulating separating flows, which we assumed to be present in the current problem in the form of dynamic stall. The SA model was shown by Ferreira et al.³⁶ to match experimental particle image velocimetry (PIV) results for a CFT in dynamic stall, though this was a somewhat low Reynolds number case (5×10^4). Further justification for using the SA model for this case comes from Crivellini and D’Alessandro³⁷, where they successfully modeled the laminar separation bubble and subsequent boundary layer transition to turbulence at Reynolds numbers similar to those investigated here.

A. Computational mesh

The computational domain was a rectangular volume 3.66 m long, 3.66 m wide, and 2.44 m tall (for 3-D), with the turbine located 1.52 m from the inlet, and centered vertically with a vertical axis, designed to match the tow tank dimensions for comparison with previous experiments. The rotor geometry was located at the center of a cylindrical sliding mesh

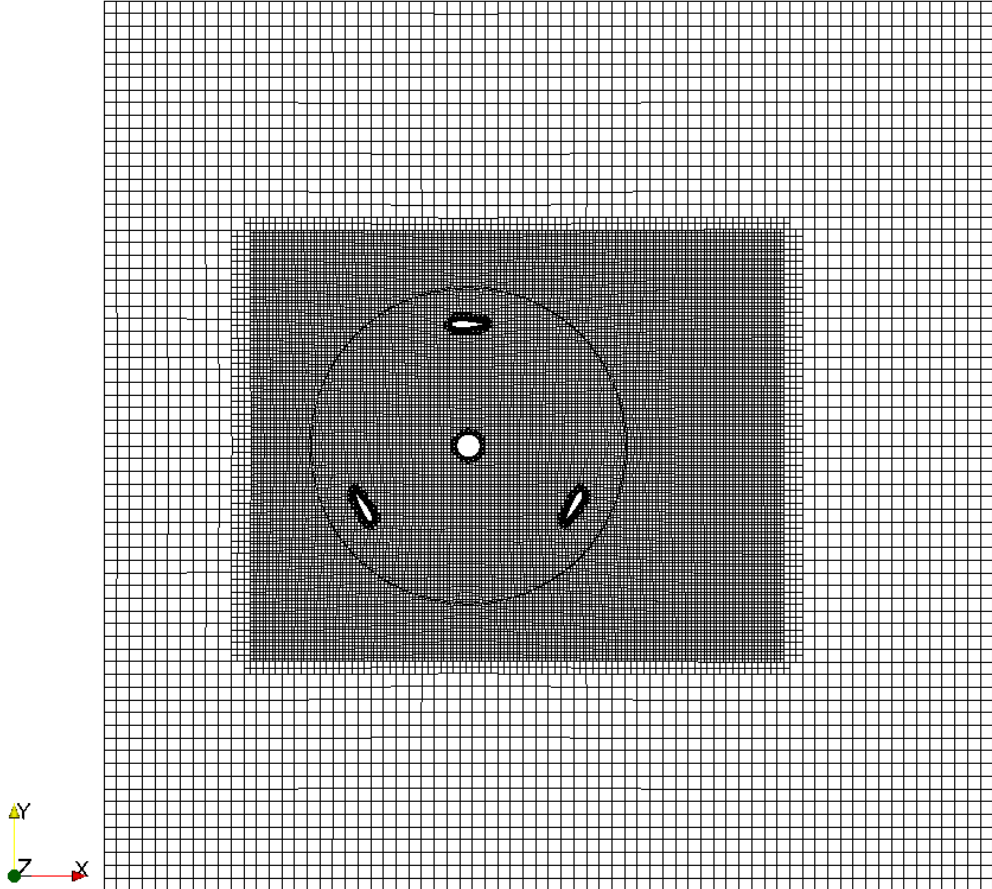


FIG. 3: Overview of the 2-D computational mesh.

interface, which rotated at a mean tip speed ratio $\lambda = 1.9$ with a sinusoidal oscillation at the blade passage frequency—with an amplitude of 0.19 and the first peak at 1.4 radians—to mimic the slight deviation from the mean tip speed ratio observed in the experiments. The 2-D mesh overview is shown in Figure 3 and the blade mesh detail is shown in Figure 4.

Meshes were generated using *OpenFOAM*'s *blockMesh* and *snappyHexMesh* utilities. Mesh topology consists of a background hexahedral mesh, which is refined in all three directions by a factor of 2 in a rectangular region containing the turbine and near-wake (0.9 m upstream, 1.3 m downstream, ± 0.9 m cross-stream, and ± 0.8 m vertically). Cells adjacent to the turbine shaft and struts are refined by a factor of 4, while cells adjacent to the blades are refined by a factor of 6. To capture the boundary layer, 20 layers are added next to the blades with an expansion ratio of 1.2. Overall mesh refinement is controlled by a single parameter—the number of cells in the streamwise direction, N_x .

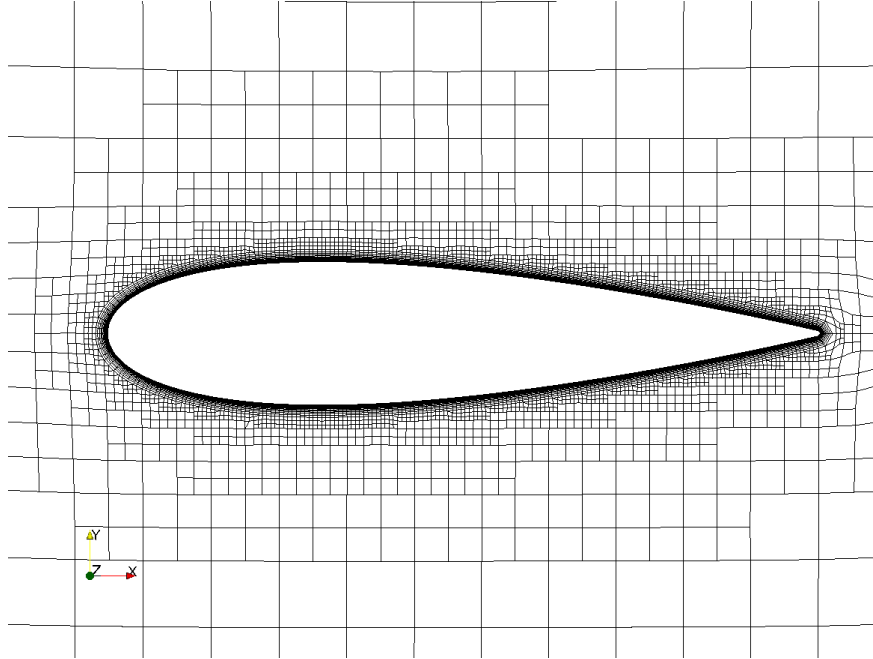


FIG. 4: Detailed view of the 2-D computational mesh near the blades.

B. Solver

Simulations were run using the *pimpleDyMFoam* solver from the open-source finite volume CFD package *OpenFOAM*, version 2.3.x. *pimpleDyMFoam* uses a hybrid PISO-SIMPLE algorithm for pressure-velocity coupling and is compatible with dynamic meshes. An Euler scheme was used to advance the simulation forward in time. The case files required to replicate the simulations are available from³⁸⁻⁴¹.

C. Initial and boundary conditions

Initial and boundary conditions were set to match those of the tow tank as well as possible. The velocity at the inlet, bottom, and side walls was fixed to 1 m/s to match the tow tank case, while the top boundary condition was a slip velocity condition. Pressure was held fixed at the outlet. Note that in 2-D the top and bottom boundary conditions are “empty,” which is an OpenFOAM convention to indicate two-dimensionality.

Since the mesh was only refined next to the blade surfaces in order to resolve the boundary layer profile, no wall functions were used. However, wall functions were used for the other turbine surfaces, i.e., struts, hub, and shaft, and for the tank sidewalls, bottom, and top.

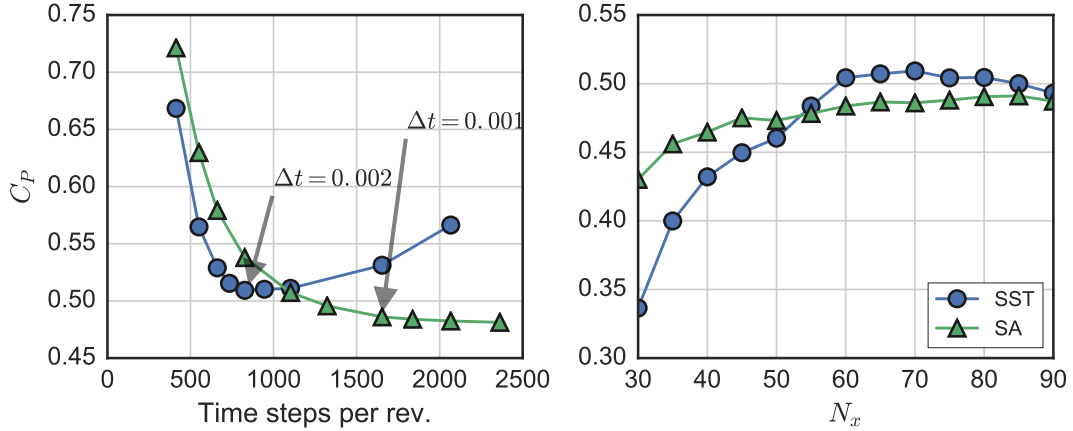


FIG. 5: Time step (left) and grid size (right) dependence for the 2-D case with both the SST and SA turbulence models. Time step dependence was carried out with $N_x = 70$ and grid size dependence with the time steps annotated for each turbulence model.

III. MODEL VERIFICATION

Both the $k-\omega$ SST and Spalart–Allmaras RANS model cases were verified for convergence of the turbine mean power coefficient with respect to grid spacing and time step using 2-D domains. The grid topology was fixed, but the number of cells per domain length was scaled proportionally, maintaining the same background mesh cell aspect ratio. Results for this parameter sweep are shown in Figure 5, from which the final number of streamwise grid points $N_x = 70$ was chosen. This corresponds to a total cell count of approximately 5×10^4 for the 2-D cases and 16 million for the 3-D case.

Time step dependence was evaluated using the 2-D $N_x = 70$ grid, the results from which are shown in Figure 5. It was seen that the Spalart–Allmaras model converged well with decreasing time step, leading to a final time step of 0.001 s. The results from the SST model show a local minimum at $\Delta t = 0.002$ s, with some divergence for smaller time steps. The local minimum was chosen as the final time step to run the simulations. Note that the SST model’s convergence behavior may be due to its specific implementation in *OpenFOAM*, and not indicative of the nature of the model equations. Verification studies for CFTs with this level of detail in the literature are not common, though the final time step is comparable to others⁸.

IV. RESULTS

Turbine operation in all cases was simulated for 10 seconds, or approximately six rotor revolutions. Computations for the 3-D cases were run on 192 processes (24 nodes \times 8 cores each) and took on the order of 1,000 CPU hours per second of simulated time. The 2-D simulations were run on a single processor and took on the order of one CPU hour per second.

Flow statistics were calculated over the time interval spanning 5–10 seconds, or approximately three rotor revolutions, from time series downsampled to 50 Hz. It is assumed that the downsampling frequency is high enough above the blade passage frequency such that differences from the variance (for computing turbulence statistics) in the original velocity will be negligible.

A. Performance prediction

Mean performance quantities—power and overall rotor drag coefficients—were calculated for the interval after two full rotor revolutions, beyond which values had reached an approximately periodic state. Predictions for both the mean rotor power and drag coefficients are shown in Figure 6. In general, the 2-D CFD cases both significantly overpredict turbine loading and therefore mechanical power output, which is likely due to their increased blockage ratio, unresolved blade end effects, and lack of blade support struts.

The 3-D simulations fair better at predicting the experimental measurements. The Spalart–Allmaras model’s mean power coefficient was 0.24 while the SST’s was 0.33, which represent a 6% under- and 30% overprediction, respectively, compared with the experiments. The apparent overprediction of rotor drag coefficient could be an effect of the experimental procedure, where the “tare drag” from the turbine mounting structure was measured without a turbine installed, then subtracted in post-processing. Technically the local flow field will have changed, and hence the tare drag will change as well.

B. Wake characteristics

Visualizations of the complex vorticity field generated by the turbine are presented for the 2-D and 3-D Spalart–Allmaras cases in Figure 8 and Figure 8, respectively. It can be

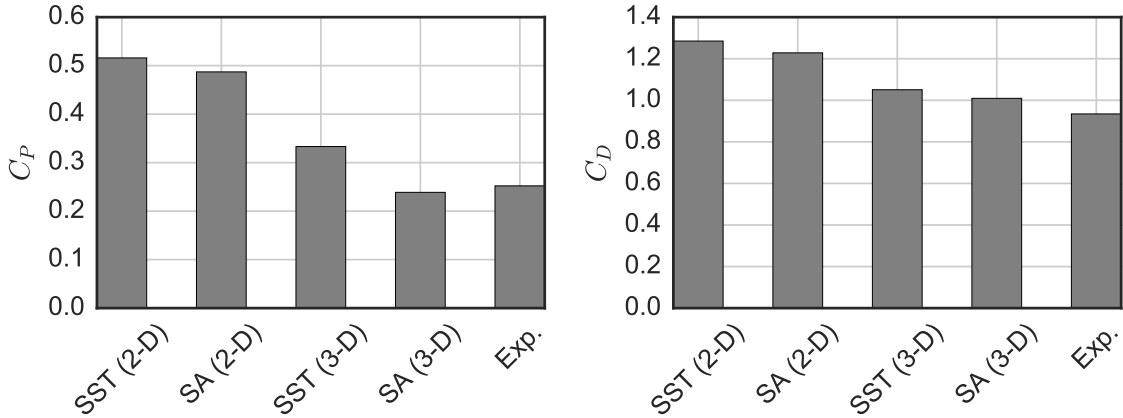


FIG. 6: Power (left) and drag (right) coefficient predictions from experiments and each numerical model.

seen how the upstream blade—as it turns back into the streamwise direction—is shedding a large amount of spanwise vorticity due to the separated flow. In the 3-D case, strong tip vortices are also present, which trace the “contracting” wake flow on the $-y$ side of the turbine associated with the induced vertical velocity field. The 3-D dynamic stall vortex also shows asymmetry about the $x-y$ mid-rotor plane; once again highlighting the importance of three-dimensional effects on wake dynamics.

Mean velocity profiles at one turbine diameter downstream are shown in Figure 9. The 2-D results suffer from a blockage mismatch, i.e., keeping the proximity of the walls constant increases the blockage ratio. The 3-D results, however, show good agreement with the experiments.

Turbulence kinetic energy profiles are also shown in Figure 9. The turbulence kinetic energy was calculated as

$$k = k_{\text{RA}} + \frac{1}{2} (\bar{U'}^2 + \bar{V'}^2 + \bar{W'}^2), \quad (1)$$

where $U' = U - \bar{U}$ and k_{RA} is the kinetic energy calculated by the turbulence model, which is zero for the SA model.

Both Spalart–Allmaras cases do a poor job predicting the turbulence kinetic energy in the flow, since it must be resolved as variance in the velocity field. The 2-D SST model does a good job predicting the peak in k at $y/R = -1$, though is missing the smaller peak at $y/R = -1$. This is once again likely due to blockage issues, where local tip speed ratio is decreased, increasing the blades’ instantaneous angle of attack at this location on the

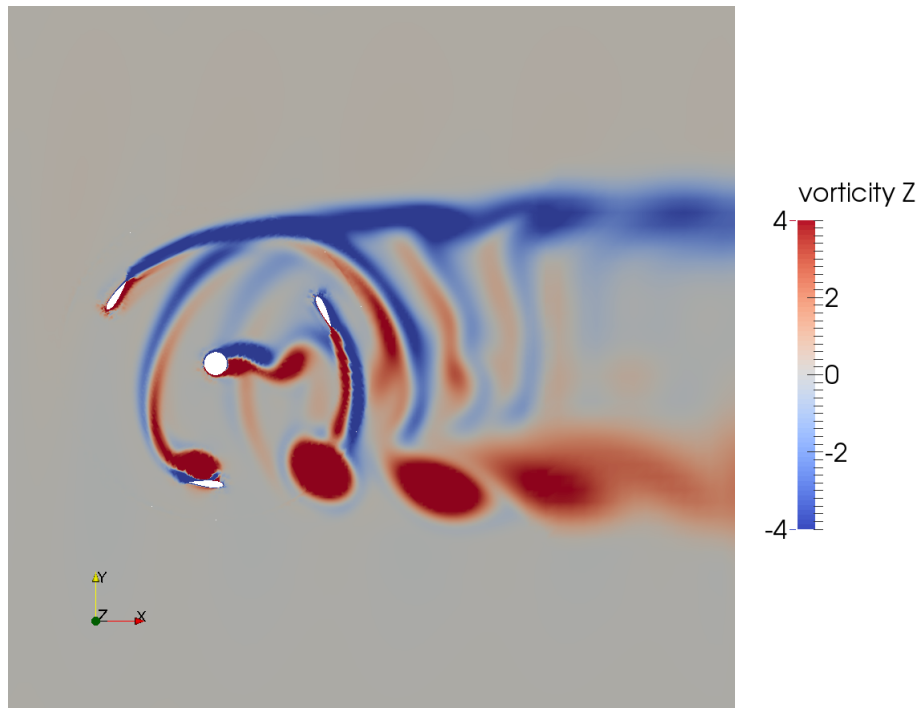


FIG. 7: Instantaneous vorticity contours (at $t = 9.64$ s) computed for the 2-D Spalart–Allmaras case.

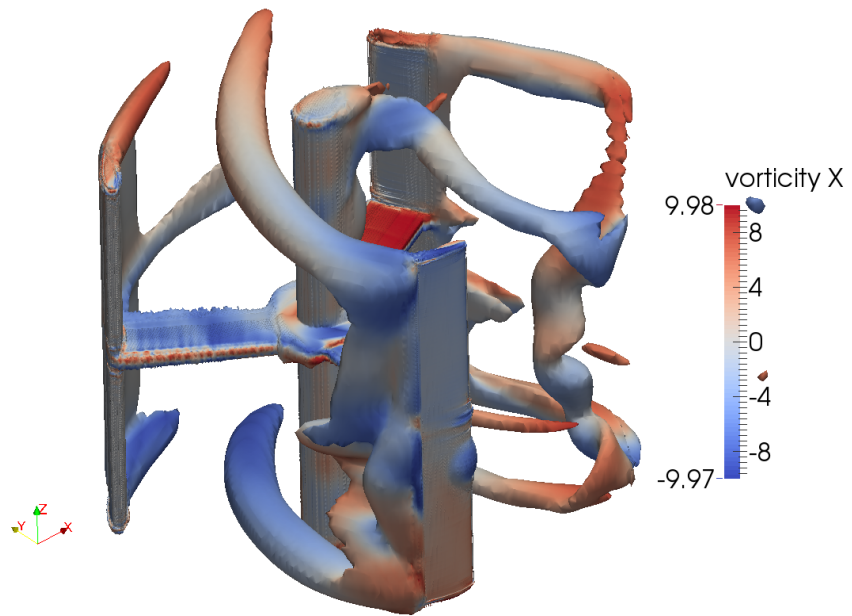


FIG. 8: Iso-vorticity contours (at $t = 9.64$ s) colored by the streamwise component of vorticity for the 3-D Spalart–Allmaras case.

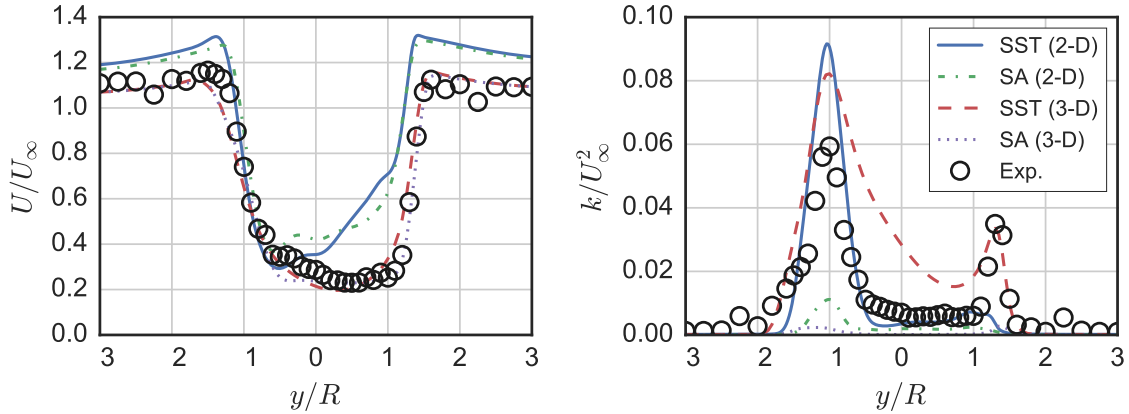


FIG. 9: Mean velocity (left) and turbulence kinetic energy (right) profiles at $x/D = 1$ from 2-D simulations, 3-D simulations ($z/H = 0$), and experiments³⁰.

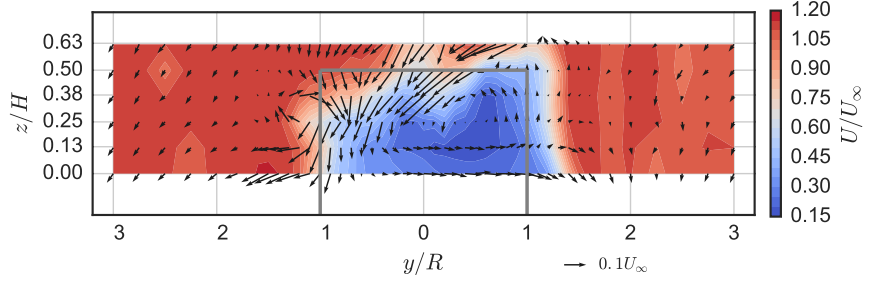
downstream passage. In contrast, the 3-D SST model predicts the $+y$ peak in turbulence kinetic energy very well, though the $-y$ peak magnitude is overpredicted by about 30%. We also see some smearing of k across the center of the rotor, which is likely due to exaggerated levels of the turbulent eddy viscosity.

1. Mean velocity in three dimensions

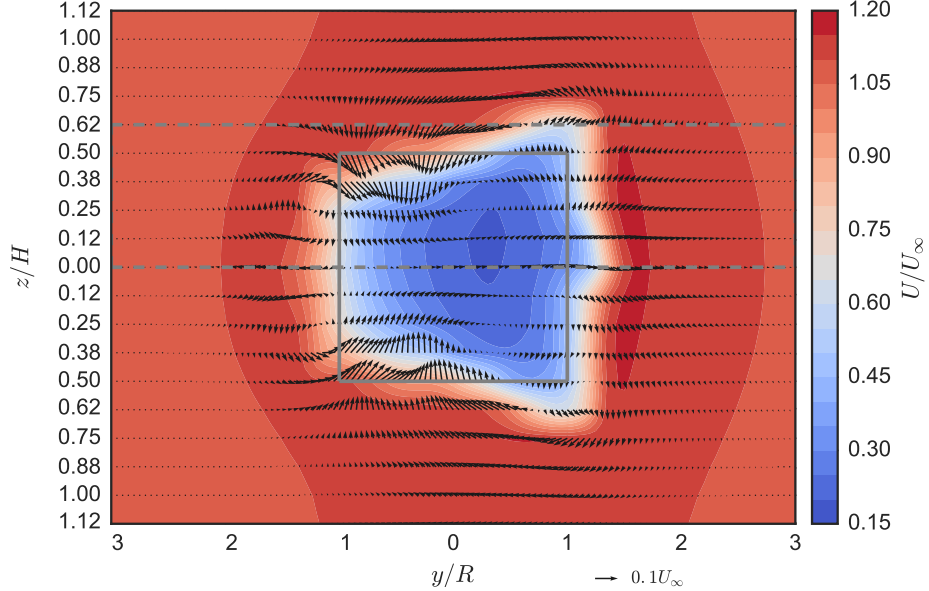
In order to visualize the mean velocity field, vector arrows for the mean cross-stream and vertical components are superimposed on top of contours of the streamwise component at $X/D = 1$ in Figure 10. Both CFD models predict the general structure of the mean velocity well, though the SA case has slightly larger vertical mean flows, which could be due to stronger tip vortex generation, or lower diffusivity compared with the SST model. Additional discrepancies between CFD and experiments may be due to the top slip boundary condition versus the experiment's free surface.

2. Turbulence kinetic energy contours

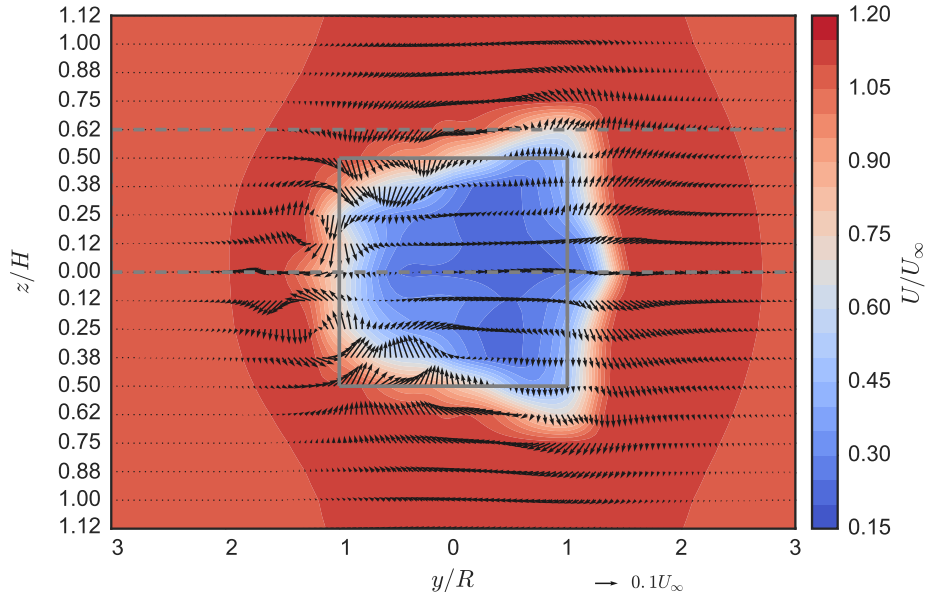
Turbulence kinetic energy contours for the experimental measurements and each CFD case at $x/D = 1$ are presented in Figure 11. As seen in the profiles in Figure 9, the SA model is resolving very little of the flow unsteadiness. In contrast, the SST model does a good



(a) Mean velocity field at $x/D = 1$ from experiments³³.

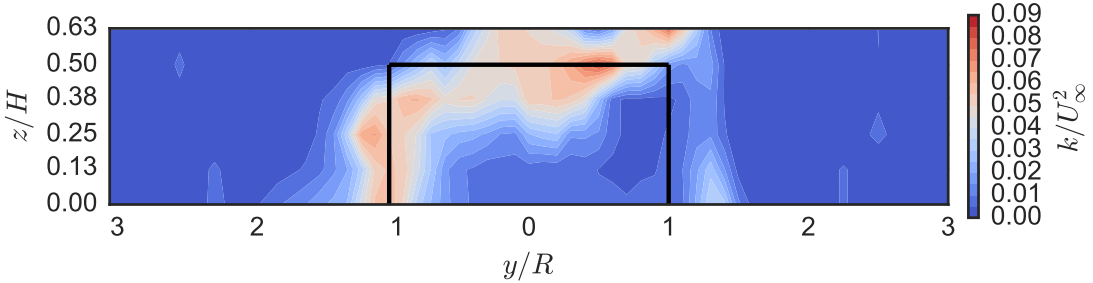


(b) Mean velocity at $x/D = 1$ computed by the 3-D SST model.

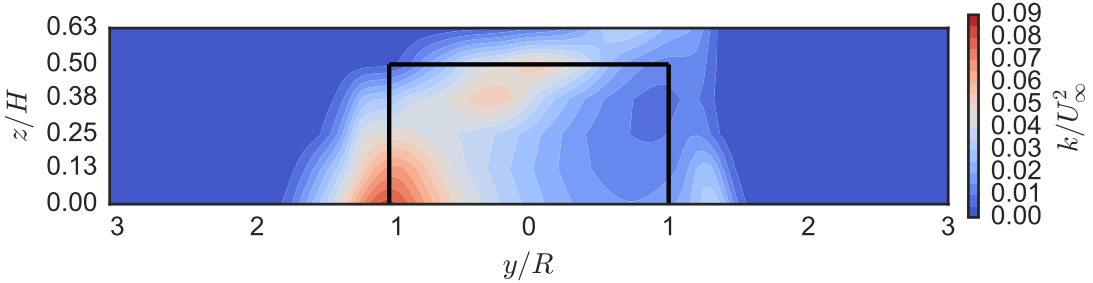


(c) Mean velocity at $x/D = 1$ computed by the 3-D SA model.

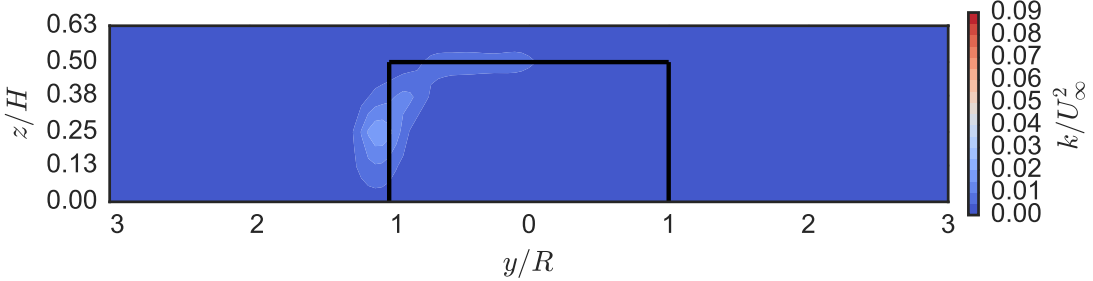
FIG. 10: Mean velocity from experiments and 3-D CFD cases. Solid gray lines indicate turbine frontal area and dashed lines indicate experimental measurement plane.
14



(a) Turbulence kinetic energy at $x/D = 1$ from experiments³³.



(b) Turbulence kinetic energy at $x/D = 1$ computed by the 3-D SST model.



(c) Turbulence kinetic energy at $x/D = 1$ computed by the 3-D SA model.

FIG. 11: Turbulence kinetic energy from experiments and 3-D CFD cases. Solid black lines indicate turbine frontal area.

job predicting the locations and magnitudes of various peaks in k . These are generated along the top of the turbine via tip vortex shedding, and the $-y$ side of the turbine via dynamic stall. We do however see the smearing effect from the dynamic stall vortex centered around $z/H = 0$, which is likely more of an issue with wake evolution rather than wake generation.

3. Momentum recovery

To get an overall idea of the wake recovery predicted by each model, we rearrange the streamwise component of the Navier–Stokes equation to isolate $\partial U/\partial x$ —following Bachant and Wosnik³⁰—and compute each term at $X/D = 1$ to compare with the experimental results.

We use the RANS models’ eddy viscosity to calculate the turbulent transport via

$$\text{Turb. trans.} = \nu_t \nabla^2 \vec{U}, \quad (2)$$

which is a different approach from those taken on the experiments, where Reynolds stresses were measured, but x -derivatives were not:

$$\text{Turb. trans. (exp.)} = - \left(\frac{\partial}{\partial y} \overline{u'v'} + \frac{\partial}{\partial z} \overline{u'w'} \right). \quad (3)$$

As such, we should not be surprised if the CFD models predict higher levels of turbulent transport than the experiments.

Normalized weighted averages for each recovery term at $x/D = 1$ are computed and multiplied by the cross-sectional area of the measurement plane, or the channel width in the 2-D cases. Results are shown in a bar chart in Figure 12. Consistent with the relatively large Reynolds number regime, viscous transport is essentially negligible compared with other mechanisms. Cross-stream advection—or the tendency of streamlines to diverge and reduce the streamwise momentum—produces a negative effect for all cases, though the 3-D SST model predicts significantly lower values. Vertical advection is by definition zero for the 2-D cases. The 3-D cases show varying results—with the SST model overpredicting and SA underpredicting the vertical velocity’s effect on replenishing streamwise momentum.

Turbulent transport and streamwise pressure gradient terms show the largest discrepancy between results. The 3-D SST case, despite doing a good job predicting turbulence kinetic energy, significantly overpredicts the turbulent transport term, while other CFD cases are comparable with the experiment. This seems to be balanced by a large adverse pressure gradient, which is also present to a smaller degree in the 3-D SA case. Interestingly, in contrast, both 2-D CFD cases create a wake where the pressure gradient is acting to slightly accelerate the flow at $x/D = 1$. Unfortunately, pressure data were not acquired from the experiment, though the 3-D delayed detached eddy simulation (DDES) of Boudreau and Dumas²¹ concur with the adverse pressure gradient condition.

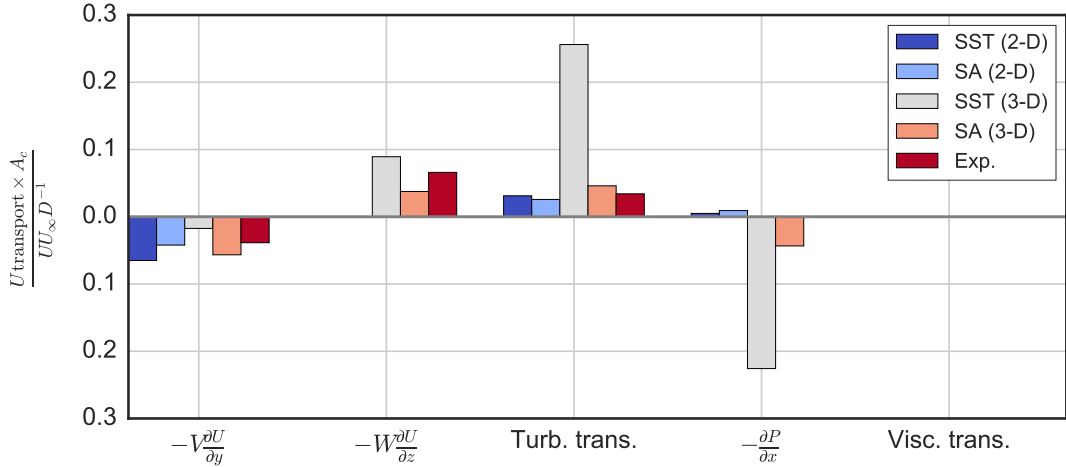


FIG. 12: Weighted sum normalized momentum recovery terms for each CFD case and experiments³³ at $x/D = 1$.

V. CONCLUSIONS

A cross-flow turbine was modeled using the $k-\omega$ SST and Spalart–Allmaras (SA) Reynolds-averaged Navier–Stokes turbulence models to test their abilities to predict turbine performance and near-wake dynamics. It was observed that when modeled in 2-D, the performance is over-predicted compared to the data from the tow tank experiments, which was expected due to omission of blade end effects, support strut drag, and increased blockage. Vertical (or axial) wake dynamics were unresolved in the 2-D model, despite being identified as a significant contributor to streamwise wake recovery, which casts doubt on the 2-D model’s applicability as a tool to study array spacing effects.

The 3-D blade-resolved RANS simulations predicted turbine performance and near-wake quite well, where the SA model results were closest to the experimentally measured performance. The SA model’s effectiveness gives hope for the prospect of replacing some physical modeling with blade-resolved CFD. However, the overprediction of power coefficient by the SST model highlights the level of technological and economic risk involved with CFD. That is to say, the SST model, despite being considered relatively trustworthy in these flow conditions, would overestimate power output by 30%.

Both the SST and SA models did a good job predicting the mean velocity field at one turbine diameter downstream, but the SST model was more effective at predicting turbu-

lence kinetic energy, since it is solved for in the turbulence model equations. Streamwise momentum recovery terms were computed from the CFD results over an entire cross-section of the domain at $x/D = 1$. Values for transport due to the mean pressure gradient and turbulent fluctuations varied a lot between the two turbulence models. Both models, however, were able to at least qualitatively resolve the vertical velocity field, which will be crucial to predicting the performance of closely spaced CFTs.

The effectiveness at predicting the mean velocity field gives credibility to the prospect of using the computed flow field to interpolate the experimental results, such that the CFD results can be used as a target for a low-order wake generator or force parameterization. These results may also help develop new tip loss corrections for blade element type models, which currently only exist for axial-flow rotors, since they provide access to the pressure and shear forces over the entire blade surface, which were not measured experimentally. Ultimately, however, the computational cost of 3-D simulations—about 10,000 CPU hours per operating case—may be too expensive to be used for CFT engineering work, especially considering the uncertainty involved compared with physical model studies. Since the 3-D wake results appeared to be only weakly asymmetrical in the x – y plane about $z/H = 0$, it may be possible to reduce computing power by only modeling the top half of the rotor and using a symmetry boundary condition at the mid-plane. However, 3-D blade-resolved RANS will likely not be practical for turbine array simulations for quite some time, and until they are, low-order models will need to be developed and improved for this purpose.

ACKNOWLEDGMENTS

The authors acknowledge funding through a National Science Foundation CAREER award (principal investigator Martin Wosnik, NSF 1150797, Energy for Sustainability, program manager Gregory L. Rorrer). The authors also thank Dr. Vincent S. Neary and the Sandia National Laboratories Water Power Program for use of their Red Mesa high performance computing cluster.

REFERENCES

¹H. J. Sutherland, D. E. Berg, and T. D. Ashwill, “A retrospective of VAWT technology,” Tech. Rep. (Sandia National Laboratories, 2012).

²I. Paraschivoiu, *Wind Turbine Design with Emphasis on Darrieus Concept*, 1st ed. (Polytechnic International, Montreal, Quebec, Canada, 2002).

³Ocean Renewable Power Company, “America’s first ocean energy delivered to the grid,” (2012).

⁴M. C. Lott, “Eiffel tower going green with two new wind turbines,” <http://blogs.scientificamerican.com/plugged-in/eiffel-tower-going-green-with-two-new-wind-turbines/> (2015).

⁵U. S. Paulsen, T. F. Pedersen, H. A. Madsen, K. Enevoldsen, P. H. Nielsen, J. Hattel, L. Zanne, L. Battisti, A. Brighenti, M. Lacaze, V. Lim, J. W. Heinen, P. A. Berthelsen, S. Carstensen, E.-J. de Ridder, G. van Bussel, and G. Tescione, “Deepwind- an innovative wind turbine concept for offshore,” in *Proceedings of EWEA* (Brussels, Belgium, 2011).

⁶Sandia National Laboratories, “Offshore use of vertical-axis wind turbines gets closer look,” (2012).

⁷J. Dabiri, “Potential order-of-magnitude enhancement of wind farm power density via counter-rotating vertical-axis wind turbine arrays,” *Journal of Renewable and Sustainable Energy* **3**, 1–13 (2011).

⁸F. Balduzzi, A. Bianchini, R. Maleci, G. Ferrara, and L. Ferrari, “Critical issues in the CFD simulation of Darrieus wind turbines,” *Renewable Energy* **85**, 419–435 (2016).

⁹R. Howell, N. Qin, J. Edwards, and N. Durrani, “Wind tunnel and numerical study of a small vertical axis wind turbine,” *Renewable Energy* **35**, 412–422 (2010).

¹⁰F. R. Menter, M. Kuntz, and R. Langtry, “Ten years of industrial experience with the sst turbulence model,” *Turbulence, Heat and Mass Transfer* **4** (2003).

¹¹A. Alaimo, A. Esposito, A. Messineo, C. Orlando, and D. Tumino, “3D CFD analysis of a vertical axis wind turbine,” *Energies* **8**, 3013–3033 (2015).

¹²P. Marsh, D. Ranmuthugala, I. Penesis, and G. Thomas, “Three-dimensional numerical simulations of straight-bladed vertical axis tidal turbines investigating power output, torque ripple and mounting forces,” *Renewable Energy* **83**, 67–77 (2015).

¹³G. W. Rawlings, *Parametric characterization of an experimental vertical axis hydro tur-*

bine, Master's thesis, University of British Columbia (2008).

¹⁴A. Orlandi, M. Collu, S. Zanforlin, and A. Shires, "3D URANS analysis of a vertical axis wind turbine in skewed flows," *J. Wind Eng. Ind. Aerodyn.* **147**, 77–84 (2015).

¹⁵R. Akins, "Measurement of surface pressure on an operating vertical-axis wind turbine," *Tech. Rep. SAND89-7051* (Sandia National Laboratories, 1989).

¹⁶S. Mertens, G. van Kuik, and G. van Bussel, "Performance of an H-Darrieus in the skewed flow on a roof," *Journal of Solar Energy Engineering* **125**, 443–440 (2003).

¹⁷H. Lam and H. Peng, "Study of wake characteristics of a vertical axis wind turbine by two- and three-dimensional computational fluid dynamics simulations," *Renewable Energy* **90**, 386–398 (2016).

¹⁸G. Tescione, D. Ragni, C. He, C. S. Ferreira, and G.J, "Near wake flow analysis of a vertical axis wind turbine by stereoscopic particle image velocimetry," *Renewable Energy* **70**, 47–61 (2014).

¹⁹M. Nini, V. Motta, G. Bindolino, and A. Guardone, "Three-dimensional simulation of a complete vertical axis wind turbine using overlapping grids," *Journal of Computational and Applied Mechanics* (2014).

²⁰L. Battisti, L. Zanne, S. Dell'Anna, V. Dossena, G. Persico, and B. Paradiso, "Aerodynamic measurements on a vertical axis wind turbine in a large scale wind tunnel," *Journal of Energy Resources Technology* **133** (2011).

²¹M. Boudreau and G. Dumas, "Wake analysis of various hydrokinetic turbine technologies through numerical simulations," in *Proceedings of AERO 2015* (2015).

²²C. Li, S. Zhu, Y. lin Xu, and Y. Xiao, "2.5d large eddy simulation of vertical axis wind turbine in consideration of high angle of attack flow," *Renewable Energy* **51**, 317–330 (2013).

²³K. W. McLaren, *A Numerical and Experimental Study of Unsteady Loading of High Solidity Vertical Axis Wind Turbines*, Ph.D. thesis, McMaster University (2011).

²⁴D. B. Araya, A. E. Craig, M. Kinzel, and J. O. Dabiri, "Low-order modeling of wind farm aerodynamics using leaky rankine bodies," *Journal of Renewable and Sustainable Energy* **6** (2014), 10.1063/1.4905127.

²⁵A. Goude and O. Agren, "Numerical simulation of a farm of vertical axis marine current turbines," in *Proceedings of the ASME 2010 29th International Conference on Ocean, Offshore and Arctic Engineering* (Shanghai, China, 2010).

²⁶N. Durrani, N. Qin, H. Hameed, and S. Khushnood, “2d numerical analysis of a vawt wind farm for different configurations,” in *Proceedings of 49th AIAA Aerospace Sciences Meeting including the New Horizons Forum and Aerospace Exposition*, AIAA 2011-461 (Orlando, FL, 2011).

²⁷S. Giorgetti, G. Pellegrini, and S. Zanforlin, “CFD investigation on the aerodynamic interferences between medium-solidity Darrieus vertical axis wind turbines,” *Energy Procedia* **81**, 227–239 (2015).

²⁸Y. Li and S. M. Calisal, “Modeling of twin-turbine systems with vertical axis tidal current turbines: Part I—power output,” *Ocean Engineering* **37**, 627–637 (2010).

²⁹S. Antheaume, T. Matre, and J.-L. Achard, “Hydraulic darrieus turbines efficiency for free fluid flow conditions versus power farms conditions,” *Renewable Energy* **33**, 2186–2198 (2008).

³⁰P. Bachant and M. Wosnik, “Characterising the near-wake of a cross-flow turbine,” *Journal of Turbulence* **16**, 392–410 (2015).

³¹P. Bachant and M. Wosnik, “Reynolds number dependence of cross-flow turbine performance and near-wake characteristics,” in *Proceedings of the 2nd Marine Energy Technology Symposium METS2014* (Seattle, WA, 2014).

³²P. Bachant and M. Wosnik, “Effects of reynolds number on the energy conversion and near-wake dynamics of a high solidity vertical-axis cross-flow turbine,” *Energies* **9** (2016), 10.3390/en9020073.

³³P. Bachant and M. Wosnik, “UNH-RVAT Reynolds number dependence experiment: Reduced dataset and processing code,” *figshare*. <http://dx.doi.org/10.6084/m9.figshare.1286960> (2016).

³⁴F. Menter, “Two-equation eddy-viscosity turbulence models for engineering applications,” *AIAA Journal* **32**, 1598–1605 (1994).

³⁵P. Spalart and S. Allmaras, “A one-equation turbulence model for aerodynamic flows,” *Tech. Rep. AIAA-92-0439* (American Institute for Aeronautics and Astronautics, 1992).

³⁶C. S. Ferreira, H. Bijl, G. van Bussel, and G. van Kuik, “Simulating dynamic stall in a 2d vawt: Modeling strategy, verification and validation with particle image velocimetry data,” *Journal of Physics: Conference Series*, The Science of Making Torque from Wind **75**, 1–13 (2007).

³⁷A. Crivellini and V. D’Alessandro, “Spalartallmaras model apparent transition and rans

simulations of laminar separation bubbles on airfoils,” International Journal of Heat and Fluid Flow **47**, 70–83 (2014).

³⁸P. Bachant, “UNH-RVAT-2D-OpenFOAM: v1.0.0-SST,” Zenodo. <http://dx.doi.org/10.5281/zenodo.47928> (2016).

³⁹P. Bachant, “UNH-RVAT-2D-OpenFOAM: v1.0.0-SA,” Zenodo. <http://dx.doi.org/10.5281/zenodo.47929> (2016).

⁴⁰P. Bachant, “UNH-RVAT-3D-OpenFOAM: v1.0.0-SST,” Zenodo. <http://dx.doi.org/10.5281/zenodo.47926> (2016).

⁴¹P. Bachant, “UNH-RVAT-3D-OpenFOAM: v1.0.0-SA,” Zenodo. <http://dx.doi.org/10.5281/zenodo.47927> (2016).